Title

Automated in Vivo Assessment of Vascular Response to Radiation Using a Hybrid Theranostic X-Ray Irradiator/Fluorescence Molecular Imaging System

Authors

Nouizi, Farouk

Brooks, Jamison

Zuro, Darren M

et al.

Publication Date

2020

DOI

10.1109/access.2020.2994943

Peer reviewed

HHS Public Access

Author manuscript

IEEE Access. Author manuscript; available in PMC 2020 June 15.

Published in final edited form as:

IEEE Access. 2020 ; 8: 93663–93670. doi:10.1109/access.2020.2994943.

Automated in vivo Assessment of Vascular Response to Radiation using a Hybrid Theranostic X-ray Irradiator/ Fluorescence Molecular Imaging System

Farouk Nouizi[1,#], **Jamison Brooks**[2,3,#], **Darren M. Zuro**[2,3], **Srideshikan Sargur Madabushi**[2], **Dayson Moreira**[4], **Marcin Kortylewski**[4], **Jerry Froelich**[5], **Lydia M. Su**[1], **Gultekin Gulsen**[1], **Susanta K. Hui**[2]

[1]Tu and Yuen Center for Functional Onco-Imaging, Department of Radiological Sciences, University of California Irvine, Irvine, CA 92697 USA.

[2]Department of Radiation Oncology, Beckman Research Institute, City of Hope National Medical Center, Duarte, CA 91010 USA.

[3]Department of Radiation Oncology, University of Minnesota, Minneapolis, MN 55455 USA.

[4]Department of Immuno-Oncology, Beckman Research Institute at City of Hope, Duarte, CA 91010 USA.

[5]Department of Radiology, University of Minnesota, Minneapolis, MN

Abstract

Hypofractionated stereotactic body radiotherapy treatments (SBRT) have demonstrated impressive results for the treatment of a variety of solid tumors. The role of tumor supporting vasculature damage in treatment outcome for SBRT has been intensely debated and studied. Fast, non-invasive, longitudinal assessments of tumor vasculature would allow for thorough investigations of vascular changes correlated with SBRT treatment response. In this paper, we present a novel theranostic system which incorporates a fluorescence molecular imager into a commercial, preclinical, microCT-guided, irradiator and was designed to quantify tumor vascular response (TVR) to targeted radiotherapy. This system overcomes the limitations of single-timepoint imaging modalities by longitudinally assessing spatiotemporal differences in intravenously-injected ICG kinetics in tumors before and after high-dose radiation. Changes in ICG kinetics were rapidly quantified by principle component (PC) analysis before and two days after 10 Gy targeted tumor irradiation. A classifier algorithm based on PC data clustering identified pixels with TVR. Results show that two days after treatment, a significant delay in ICG clearance as measured by exponential decay (40.5±16.1% P=0.0405 Paired t-test n=4) was observed. Changes in the mean normalized first and second PC feature pixel values (PC1 & PC2) were found (P=0.0559, 0.0432 paired t-test), suggesting PC based analysis accurately detects changes in ICG kinetics. The PC based classification algorithm yielded spatially-resolved TVR maps. Our first-of-its-kind theranostic system, allowing automated assessment of TVR to SBRT, will be used to better understand the role of tumor perfusion in metastasis and local control.

Corresponding author: Farouk Nouizi (fnouizi@uci.edu), Susanta K. Hui (shui@coh.org).
[#]indicates equal work was performed

Keywords

Fluorescence Molecular Imaging; Pharmacokinetics; Principal Component Analysis; Radiation Therapy; Tumor Vascular Response; Stereotactic Body Radiotherapy Treatments; Preclinical Imaging; Theranostics

I. INTRODUCTION

The tumor vasculature is a critical component of the tumor microenvironment and is responsible for nutrition and oxygen supply to regions of malignant growth [1]. In addition to oxygen and nutrient supply, the tumor vasculature plays a direct role in supporting metastasis by allowing tumor cells to enter the blood and circulate to different regions of the body [2]. During tumor development, vasculature becomes spatially heterogeneous due to the uncontrolled growth of tumor cells and angiogenic signaling [3]. The heterogeneous distribution of tumor blood vessels and physical changes of tumor vasculature result in abnormal blood perfusion compared to non-malignant vasculature [4]. How the tumor vasculature contributes to disease progression and how vascular changes during treatment affect treatment outcomes are areas of intense study.

Stereotactic body radiotherapy treatment (SBRT) uses a reduced number of treatment fractions at higher doses (hypofractionation), typically 10-20 Gy/fraction to treat solid tumors. Compared to conventional fractionation, hypofractionation has significantly decreased the relative risk of local tumor progression for patients with squamous, non-small cell lung cancer resulting in a 27% reduction in relative risk of local progression [5]. Additionally, SBRT has been shown to be tolerable and effective in patients for a variety of solid tumor cancers [6]. There has recently been much debate over whether the traditional linear quadratic model, which assumes cell death arises from ionizing radiation based DNA damage, adequately accounts for the success of SBRT or whether tumor vascular damage contributes to indirect tumor cell death through a loss of blood supply to the tumor [7]–[10]. Histological evaluations have provided evidence for extensive vascular damage following SBRT treatment, however histology is unable to perform non-invasive longitudinal assessments directly measuring blood perfusion. Since tumor recurrence with SBRT is still a common problem, longitudinal assessments of blood perfusion would be desirable because they would allow for direct correlation between tumor vascular response (TVR) and treatment outcome over time. Additionally, while the evaluation of the whole tumor is needed due to vascular heterogeneity, it is time consuming when analyzed by histology. Fast, low-cost, non-invasive techniques that allow for whole tumor measurements of vascular function would be able to correlate TVR to treatment response. This would enable TVR to be investigated as a prognostic factor for treatment outcome in SBRT and enable a better understanding of the role of TVR in SBRT tumor control.

One such technique that is well suited to obtain measurements of tumor blood perfusion is near-infrared fluorescence imaging [11], [12], which is able to image the vascular system in vivo and estimate its functional perfusion [13]–[15]. In particular, dynamic fluorescence imaging (DynFI), which is based on time-series analysis of a given fluorescent probe's pharmacokinetics, can be used to accurately and quantitatively measure functional

parameters such as perfusion rate and vascular permeability for many clinical and preclinical applications [16]–[21]. A fluorescent agent commonly used for DynFI is indocyanine green (ICG). After injection, ICG rapidly binds to albumin making the kinetics of ICG fully governed by the temporal dynamics of albumin in vivo [22]. Using the FDA approved near-Infrared fluorescent agent ICG, DynFI has been used to characterize perfusion and vascular permeability in solid tumors making it suitable for monitoring TVR in SBRT tumor treatments [23], [24].

Acquiring spatiotemporal DynFI data using CCD camera-based systems typically yields extremely large data sets (i.e., number of pixels x dynamic time points) that require time consuming analysis. This hampers the practical application of this technique [25]. Analysis time can often be shortened by temporal or spatial dimension reduction. Typically, temporal dimension reduction is achieved through extraction of important temporal features (blood flow index, perfusion rate, mean transit time, etc.) that characterize pharmacokinetics [19]. However, the use of these temporal features is limited by their susceptibility to noise and motion artifacts [21]. Spatial dimension reduction of DynFI data is usually achieved by averaging DynFI signals within the tumor region, discarding any spatial information. A more elegant way to assess the entire DynFI spatiotemporal data is to extract pixel-specific pharmacokinetic signatures by using principle component analysis (PCA) [21], [25]–[29]. Analysis using PCA can be performed using pharmacokinetics of a wide variety of imaging agents in many tissues. PCA enables a rapid automated analysis of longitudinal data to quantitatively measure TVR, while still preserving spatial information.

In this paper, we describe a first-of-its-kind theranostic CCD-based DynFI/microCT-guided targeted irradiator that longitudinally assesses TVR to SBRT treatments in tumor bearing mice. A rapid, automated data analysis method using PCA of the spatiotemporal data is used to extract pharmacokinetic information of ICG. Differences in the first and second principle component feature (PC1 & PC2) of ICG pharmacokinetics were found in tumors immediately before and two days after 10 Gy SBRT. The dose of 10 Gy was chosen as early changes in tumor vasculature have been seen at a wide range of doses (5-20 Gy/fraction) [30], [31]. Pretreatment and posttreatment data were plotted as a scatterplot in PC1-PC2 space and a classification algorithm based on a 99.9% confidence covariance ellipse was used to identify responding (TVR_{pos}) and non-responding (TVR_{neg}) tumor pixels for rapid spatial mapping of tumor heterogeneity. Results demonstrate the ability of the theranostic system to both observe changes in ICG pharmacokinetics and perform fast, automated assessments of vascular response to SBRT.

II. MATERIALS AND METHODS

A. ANIMAL AND TUMOR MODEL

Four 10-15 week old C57/B6 mice (Strain 000664, The Jackson Laboratory) were subcutaneously injected in the right thigh muscle with aggressive murine oral cavity cancer, MOC2 cells (1×10^5 cells) [32] suspended in phosphate buffered saline (100 μl). Mice were injected 21 days before the start of imaging and treatment. Before imaging, the hair on the thighs and backs of the mice was removed using hair depilatory cream (Church & Dwight Company). During the treatment and imaging sessions, mice were anesthetized initially with

3% isoflurane mixed with O_2 at a flow rate of 2 L/min, then maintained with 1.5% isoflurane at an O_2 flow rate of 1.5 L/min. For imaging, an intravenous catheter was inserted into the tail vein to administer ICG (4.7 μg, approximately 0.19 mg/kg) suspended in saline (75 μl) during image acquisition. Pretreatment imaging was acquired just prior to radiation treatments. All mice fully recovered after the imaging procedure. Tumors volumes were measured before and two days after treatment by calipers. Tumor volume was calculated using the formula volume = length *width^2/2. All animal experiments were performed according to City of Hope guidelines and approved by the Institutional Animal Care and Use Committee.

B. INSTRUMENTATION AND DynFI DATA ACQUISITION

The theranostic system was built by incorporating a CCD-based fluorescence molecular imaging (FMI) system [33] into a commercial preclinical X-ray CT image-guided radiation therapy platform (X-RAD SmART, Precision X-Ray, Inc.). The FMI system uses a 785 nm laser diode (75 mW, Thorlabs) for ICG excitation. The laser diode mounts and drivers were integrated into the system gantry (Fig. 1). The drivers were operated in constant power mode to ensure output stability during the experiments. The laser output was collimated then sent towards an illumination point below the mouse using a galvano-mirror scanner. A cooled CCD camera (Perkin Elmer, Cold Blue) was positioned directly above the mouse to perform transillumination data acquisition. A sigma MACRO 50 mm F2.8 lens was coupled to the CCD camera, providing 2280 pixels × 1528 pixels images. The pixels were binned during acquisition using a factor of 4, resulting in 570 pixels × 382 pixels images with a pixel size of 0.2 mm × 0.2 mm. A computer-controlled filter-wheel (Tofra, Inc.) was installed between the CCD camera body and the lens. Two 830 nm band-pass filters (MK Photonics) were stacked and used to eliminate excitation light at 785 nm. This filter combination was used to minimize the strong excitation leakage with a maximum transmission rate at the fluorophore emission wavelength (830 nm).

A DynFI series of 46 images was acquired with an integration time of 10 seconds per frame. ICG was injected at the start of acquisition of the 5th frame. The four frames acquired before ICG injection were averaged and used as baseline, which was subtracted from the remaining 42 DynFI images. This was used to correct for both the residual fluorescence signals and the excitation light leakage through the rejection filters [34].

C. MicroCT IMAGE ACQUISITION AND SBRT TREATMENT

The X-ray irradiation was performed using the preclinical X-ray microCT image-guided radiation therapy platform (X-RAD SmART). MicroCT images were acquired (0.1 mm × 0.1 mm) using a low-dose of radiation ($\ll$10 Gy). After CT images were acquired, a Monte Carlo-based planning treatment simulation tool was used to establish and deliver the optimal image-guided 10 Gy treatment to the tumor region of interest (ROI).

D. KINETICS FEATURES EXTRACTION AND VISUALIZATION

PCA was performed using the “pca” Matlab® function, on the DynFI fluorescence signals within the tumor ROI and kidney ROI. Before quantifying the induced PC variation, the pretreatment and posttreatment pixel PC feature values were normalized by subtracting their

corresponding mean pretreatment PC feature value. An RGB image was made by assigning the normalized PC1 and PC2 feature values to the red channel and blue channels, respectively [25]. The green channel was set to zero. Each of the channels was individually converted to gray scale using the “mat2gray” Matlab® function then normalized to 255. Finally, the ROIs of the resulting PC-RGB image were superimposed on the corresponding gray scale ambient-light images.

E. DATA REPRESENTATION AND STATISTICS

The 99.9% confidence covariance ellipse is defined based on the covariance of data. Its two major axes are calculated from the two-dominant data eigenvectors, while their magnitude corresponds to data eigenvalues. The orientation of the ellipse is given by the angle between the major eigenvector and the x-axis.

Significance measurements were calculated using Prism (V.7.01, GraphPad). A p-value of 0.05 or lower was considered significant. For box and whisker plots, boxes represent the 25^{th} and 75^{th} percentile, and error bars indicate the min and max of the data. All paired t-tests are performed using two-sided difference based statistical testing.

III. RESULTS

A. SBRT-INDUCED CHANGES IN PHARMACOKINETICS OF ICG

To monitor and quantify TVR after high-dose irradiation, we acquired a series of 46 DynFI images before and 48 h post-irradiation of the tumor. The DynFI fluorescence images were presented in logarithmic scale because of their large gray-level dynamic range (Fig. 2a,c). We first analyzed the DynFI images simply using mean dynamic fluorescence signals obtained over the tumor ROI. Tumor ROI’s from pre and two days posttreatment imaging were automatically segmented on the respective pre and posttreatment microCT images. The multimodal system is fully integrated enabling fast, accurate and automated co-registration of DynFI and microCT ROIs.

A delay in both tumor uptake and tumor clearance of ICG two days after SBRT treatment can be observed (Fig. 2b), while no such delays are observed in the kidney (Fig. 2d). Additionally, the size of tumors did not change during treatment (336.1±152.7 and 320.9±155.7 mm^2, P = 0.5971 Paired t-test) suggesting any changes in ICG kinetics were related to tumor biology rather than tumor geometry changes. Post-irradiation tumor ICG kinetics showed a slight delay during the ICG uptake compared to the pre-irradiation kinetics. However, a considerable delay was seen in the ICG clearance from the tumor. Significant increases in averaged ICG retention was observed in tumors, resulting in a 40.5±16.1% decrease in the exponential decay parameter of ICG after it had reached peak concentration (P = 0.0405 Paired t-test n = 4). As control, we analyzed the DynFI signal from the left kidney. The kidney ROI was determined by comparison to an open source mouse atlas [35]. No significant variation in the half-life of ICG decay was seen for the kidney ROI (Fig. 2d). This suggests that changes in ICG dynamics of the tumor after treatment are due to vascular damage with SBRT therapy [36].

B. SBRT-INDUCED CHANGES IN THE PRINCIPLE COMPONENTS

Taking DynFI pixel data (Fig. 3a,c), we obtained a simplified spatiotemporal feature representation by PCA analysis. Only the first two projected PC features (PC1 and PC2) were evaluated, as they were shown to be proportional to the area under the kinetic curve and to the exponential decay parameter of ICG, respectively [21]. Additional PC features were discarded since they were sensitive to image noise and have not been shown to directly represent ICG kinetics [21]. Spatial mapping of the DynFI spatiotemporal pharmacokinetics of ICG using PC space mapping allowed for a straight-forward observation of SBRT-induced TVR (Fig. 3b,d). A clear change in normalized PC1 and PC2 feature values for the tumor are seen after SBRT treatment, while no change is observed for kidney (Fig. 3e,f).

Nearly significant and significant differences in mean normalized whole-tumor PC feature values were observed for PC1 ($P = 0.0559$ Paired t-test $n = 4$) and PC2 ($P = 0.0432$ Paired t-test $n = 4$) respectively (Fig. 4a-d).

C. AUTOMATED ASSESSMENT OF SBRT TVR RESPONSE

After observing distinctions between PC feature values before and after SBRT tumor treatments, we sought to create an automatic analysis process to quantify the degree of SBRT-induced TVR. To do this, pretreatment and posttreatment scatter plots of normalized PC1 and PC2 feature values were generated.

Tumor pixels were classified as non-responding, partially responding, or fully responding based on their pretreatment and posttreatment normalized PC1 and PC2 feature values unlikelihood. To perform this classification, a 99.9% confidence covariance ellipse was calculated for the pretreatment tumor pixels [37]. Posttreatment tumor pixels were identified as tumor vascular response positive (TVR_{pos}) if they were outside of the confidence ellipse or tumor vascular response negative (TVR_{neg}) if they were inside the confidence ellipse.

The classification algorithm identified mouse two as a partial-responder with 86.5% of pixels being TVR_{pos} (Fig. 5a) and mouse three was as a complete responder with 100% TVR_{pos} pixels (Fig. 5c). The spatial location of TVR_{pos} and TVR_{neg} pixels were displayed for rapid identification of TVR spatial heterogeneity (Fig. 5b,d). Results demonstrate the ability of the classification algorithm to effectively measure TVR caused by SBRT.

IV DISCUSSION AND CONCLUSION

In this work we have demonstrated the effects of SBRT on ICG tumor perfusion using longitudinal in vivo imaging and shown that SBRT leads to delayed clearance of tumor bound ICG. To our knowledge this is the first preclinical report using a multimodal theranostic system combined with automated analysis to monitor spatiotemporal TVR to SBRT. The effects of SBRT were quantified using principle component analysis in order to assess TVR heterogeneity. Significant increases in PC1 and decreases in PC2 feature values were seen in treated mice. Principle component analysis was used to identify tumor pixels as TVR_{pos} and TVR_{neg}. Data acquisition and principle component analysis could be performed right after treatment and allows for rapid treatment and imaging without moving the animal. Rapid data acquisition and analysis of early TVR will help determine whether additional

treatments are needed for tumor control. The developed system will enable correlation of TVR to metastatic and local tumor control during radiation therapy.

Dynamic Fluorescence imaging of ICG can detect changes in vascular perfusion. This is crucial in solid tumors where the efficiency of blood transport through the tumor likely contributes to the number of circulating tumor cells (CTCs) in the blood, potentially contributing to metastasis. The presence of functional tumor vasculature plays an integral role in the mobilization of CTCs [2]. The number of CTC's after radiation therapy are elevated, but significantly less in patients with hypofractionated radiation therapy compared to conventional radiation therapy [38], [39]. However the degree to which radiation therapy contributes to metastasis through the migration of irradiated tumor cells is of some debate, as irradiation has been shown to promote the growth of previously dormant metastatic clones through cellular signaling [40], [41]. Longitudinal observation of tumor vascular perfusion correlated to both CTCs and metastatic occurrence after SBRT will give further insight into this area.

The impact of vascular function on local tumor control post SBRT has recently been of much debate. Vascular damage with high-dose SBRT contributes to hypoxia and nutrient deprivation, but the degree to which this contributes to local tumor control has not been fully explored. It has been shown that high-dose single fraction SBRT has led to indirect cell death in multiple preclinical tumor types. Poor oxygen and nutrient perfusion as well as reperfusion injury have been proposed as causes of indirect cell death [9], [42]. However, other studies have observed that endothelial/stromal cell radiosensitivity had no influence on the amount of radiation needed to induce local tumor control of xenografted human tumors, but affected the regrowth rate of relapsed tumors [43]. Other studies have observed similar findings, but also found that increased tumor cell radiosensitivity resulted in increased tumor control [44], [45]. These studies demonstrate the importance of accurate measurements of vascular perfusion for radiation therapy related studies. Direct correlation between vascular perfusion and tumor control should be performed in multiple tumor types to understand the effects of radiation-induced TVR.

Current imaging modalities used to assess TVR in preclinical studies have some limitations [30]. For example, dynamic contrast-enhanced (DCE)-MRI [46] and Nuclear Imaging [47] are expensive and require constraining scheduling for longitudinal preclinical imaging studies. Although already integrated into the irradiator, CT is limited by its low sensitivity and raises dose accumulation concerns [48]. Ultrasound, is user dependent, requires direct tissue contact and dedicated instrumentation [49]. As an alternative, we have presented a simple, low-cost optical technique as an add-on to a commercial CT-guided preclinical irradiator for in vivo monitoring of the spatiotemporal TVR, filling the need for non-invasive imaging tools to assess vascular changes longitudinally and spatially across the tumor in response to SBRT.

In conclusion, DynFI imaging will allow for observations of early TVR and tumor perfusion. This will enable a better understanding of how tumor vasculature affects metastasis, tumor growth, and local tumor control. Our recent study revealed radiation-induced vascular alterations may modulate hypoxia, adversely affecting tumor control probability in

successive fractionated treatments [50]. This system will provide a novel tool to observe the complex dynamics of tumor perfusion and its impact on tumor control for conventional and hypofractionated radiation therapy.

ACKNOWLEDGMENT

The authors would like to thank Keely Walker, Ph.D. for proofreading the manuscript.

This work is supported by the National Institutes of Health (NIH) P30CA033572 (cancer center-CoH), P30CA62203 (cancer center-UCI), partly supported by other National Institutes of Health grants 1R01CA154491 (SH), R01CA215183 (MK), R21 CA191389 (GG), a City of Hope Excellence Award (SH), ONCOTEST (SH), Department of Defense grant W81XWH1910852 (MK), and the Merle and Fern Loken Professorship in Medical Physics award (JF).

Biography

FAROUK NOUIZI received the M.S. degree in Signals and Images in Medicine from University of Paris XII, Paris, France, in 2006 and the Ph.D. degree in Image, Sciences and Technology of Information (Multimodality Imaging) from University of Strasbourg, Strasbourg, France, in 2011. He is currently an Assistant Researcher in the Center for Functional Onco-Imaging, Department of Radiological Sciences, University of California at Irvine (UCI). He is the Manager of the In Vivo Functional Onco Imaging Shared Resource, Chao Family Comprehensive Cancer Center, UCI. His current research interests include the development of cutting-edge biomedical technologies and multimodality imaging techniques. He serves as a Reviewer in several specialized journals, such as IEEE Transactions on Biomedical Engineering, Journal of Biophotonics, Journal of Biomedical Optics, Optics Express, and Biomedical Optics Express.

JAMISON BROOKS is currently pursuing the Ph.D. degree in medical physics with the University of Minnesota. Since 2016, he has been with the Radiation Oncology Department, City of Hope. His current research interest includes the use of multimodal imaging to assess the response of the bone marrow to radiation and malignant disease.

DARREN M. ZURO received the M.S. degree in medical physics from the University of Arizona, in 2015. He is currently pursuing the Ph.D. degree in medical physics with the University of Minnesota. Since 2016, he has been with the Radiation Oncology Department, City of Hope. His current research interest includes applying multimodal imaging to advanced radiation treatment techniques.

SRIDESHIKAN S. MADABUSHI received the Ph.D. degree in biochemistry from the Indian Institute of Science, in 2011. He is currently a Staff Scientist in radiation oncology with the City of Hope. His postdoctoral training focused on hematopoietic stem cell biology in preclinical mouse models. His current research interests include the effect of targeted radiation on hematopoietic stem cell transplant (clinical and preclinical) and immune modulation post radiation in leukemia mouse models.

DAYSON MOREIRA received M.S. and Ph.D. degree in Pharmacology from the University of Sao Paulo, Brazil with focus in tumor biology. He is trained in tumor immunology at Beckman Institute of City of Hope. He is currently a Staff Scientist at City

of Hope. His research interests include tumor immunology, oligonucleotide-based therapy and myeloid derived suppressor cells.

MARCIN KORTYLEWSKI received the Ph.D. degree in molecular biology (Poznan University of Medical Sciences, Poland) and completed postdoctoral training in cancer biology (RWTH Aachen, Germany) as well as in tumor immunology (Moffitt Cancer Center, Tampa, FL). He is currently an Associate Professor in the Department of Immuno-Oncology at City of Hope. His research focuses on novel cancer immunotherapies using cell-selective delivery of oligonucleotides to break tumor immune tolerance.

Jerry Froelich- received his MD from West Virginia University. He is currently a Professor of Radiology with the Department of Radiology at the University of Minnesota and a practicing Radiologist at the University of Minnesota Medical Center.

LYDIA M. SU received her Ph.D. in Physics from University of California Irvine. She is currently a Professor in the Department of Radiological Sciences and the Director of John Tu & Thomas Yuen Center for Functional Onco-Imaging.

GULTEKIN GULSEN received the Ph.D. degree from Bogazici University, Istanbul, Turkey. He is currently an Associate Professor with the Departments of Biomedical Engineering and Radiology, University of California at Irvine (UC-Irvine). He is the Director of the Division of Optical Imaging, Department of Radiology, at UC-Irvine. He currently serves as the director of the In Vivo Functional Onco Imaging Shared Resource, Chao Family Comprehensive Cancer Center, UCI. His current research focuses on the development of cutting-edge multimodality imaging techniques.

SUSANTA K. HUI received the Ph.D. degree in experimental nuclear physics from Calcutta University, and the national scholarship from India. He is trained in clinical medical physics with the University of Wisconsin, Madison, WI, USA. He is currently a Professor of radiation oncology with the City of Hope. His current research interests include multimodal imaging and theranostic approaches for precision and personalized radiation medicine.

References

[1]. Hanahan D and Weinberg RA, "Hallmarks of cancer: the next generation," cell, vol. 144, pp. 646–674, 2011. [PubMed: 21376230]

[2]. Liotta LA, Kleinerman J, and Saidel GM, "Quantitative Relationships of Intravascular Tumor Cells, Tumor Vessels, and Pulmonary Metastases following Tumor Implantation," Cancer Research, vol. 34, p. 997, 1974. [PubMed: 4841969]

[3]. Nagy JA, Chang S-H, Shih S-C, Dvorak AM, and Dvorak HF, "Heterogeneity of the tumor vasculature," Seminars in thrombosis and hemostasis, vol. 36, pp. 321–331, 2010. [PubMed: 20490982]

[4]. Stylianopoulos T, Munn LL, and Jain RK, "Reengineering the Physical Microenvironment of Tumors to Improve Drug Delivery and Efficacy: From Mathematical Modeling to Bench to Bedside," Trends in Cancer, vol. 4, pp. 292–319, 2018. [PubMed: 29606314]

[5]. Saunders M, Dische S, Barrett A, Harvey A, Griffiths G, and Parmar M, "Continuous, hyperfractionated, accelerated radiotherapy (CHART) versus conventional radiotherapy in non-small cell lung cancer: mature data from the randomised multicentre trial," Radiotherapy and Oncology, vol. 52, pp. 137–148, 1999/08/01/ 1999. [PubMed: 10577699]

[6]. Brown JM and Koong AC, "High-Dose Single-Fraction Radiotherapy: Exploiting a New Biology?," International Journal of Radiation Oncology*Biology*Physics, vol. 71, pp. 324–325, 2008/06/01/ 2008.

[7]. Sperduto PW, Song CW, Kirkpatrick JP, and Glatstein E, "A hypothesis: indirect cell death in the radiosurgery era," Int J Radiat Oncol Biol Phys, vol. 91, pp. 11–3, 1 1 2015. [PubMed: 25835617]

[8]. Song CW, Park I, Cho LC, Yuan J, Dusenbery KE, Griffin RJ, et al., "Is indirect cell death involved in response of tumors to stereotactic radiosurgery and stereotactic body radiation therapy?," Int J Radiat Oncol Biol Phys, vol. 89, pp. 924–5, 7 15 2014. [PubMed: 24969800]

[9]. Song CW, Cho LC, Yuan J, Dusenbery KE, Griffin RJ, and Levitt SH, "Radiobiology of stereotactic body radiation therapy/stereotactic radiosurgery and the linear-quadratic model," Int J Radiat Oncol Biol Phys, vol. 87, pp. 18–9, 9 1 2013. [PubMed: 23608235]

[10]. Brown JM, Carlson DJ, and Brenner DJ, "The tumor radiobiology of SRS and SBRT: are more than the 5 Rs involved?," Int J Radiat Oncol Biol Phys, vol. 88, pp. 254–62, 2 1 2014. [PubMed: 24411596]

[11]. Frangioni JV, "In vivo near-infrared fluorescence imaging," Current Opinion in Chemical Biology, vol. 7, pp. 626–634, 2003. [PubMed: 14580568]

[12]. Sevick-Muraca E, "Translation of near-infrared fluorescence imaging technologies: emerging clinical applications," Annual review of medicine, vol. 63, pp. 217–231, 2012.

[13]. Marshall MV, Rasmussen JC, Tan I-C, Aldrich MB, Adams KE, Wang X, et al., "Near-infrared fluorescence imaging in humans with indocyanine green: a review and update," Open surgical oncology journal (Online), vol. 2, p. 12, 2010. [PubMed: 22924087]

[14]. Hong G, Diao S, Chang J, Antaris AL, Chen C, Zhang B, et al., "Through-skull fluorescence imaging of the brain in a new near-infrared window," Nature Photonics, vol. 8, p. 723, 2014. [PubMed: 27642366]

[15]. Hong G, Lee JC, Jha A, Diao S, Nakayama KH, Hou L, et al., "Near-infrared II fluorescence for imaging hindlimb vessel regeneration with dynamic tissue perfusion measurement," Circulation: Cardiovascular Imaging, vol. 7, pp. 517–525, 2014. [PubMed: 24657826]

[16]. Keller E, Wolf M, Martin M, and Yonekawa Y, "Estimation of cerebral oxygenation and hemodynamics in cerebral vasospasm using indocyaningreen dye dilution and near infrared spectroscopy: a case report," Journal of neurosurgical anesthesiology, vol. 13, pp. 43–48, 2001. [PubMed: 11145478]

[17]. Leung TS, Tachtsidis I, Tisdall M, Smith M, Delpy DT, and Elwell CE, "Theoretical investigation of measuring cerebral blood flow in the adult human head using bolus Indocyanine Green injection and near-infrared spectroscopy," Applied optics, vol. 46, pp. 1604–1614, 2007. [PubMed: 17356602]

[18]. Fischer T, Ebert B, Voigt J, Macdonald R, Schneider U, Thomas A, et al., "Detection of rheumatoid arthritis using non-specific contrast enhanced fluorescence imaging," Academic radiology, vol. 17, pp. 375–381, 2010. [PubMed: 19969473]

[19]. Kang Y, Lee J, An Y, Choi C, and Jeon J, "Segmental analysis of indocyanine green pharmacokinetics for the reliable diagnosis of functional vascular insufficiency," Journal of biomedical optics, vol. 16, p. 030504, 2011. [PubMed: 21456859]

[20]. Kang Y, Lee J, Kwon K, and Choi C, "Dynamic fluorescence imaging of indocyanine green for reliable and sensitive diagnosis of peripheral vascular insufficiency," Microvascular research, vol. 80, pp. 552–555, 2010. [PubMed: 20637783]

[21]. Seo J, An Y, Lee J, Ku T, Kang Y, Ahn CW, et al., "Principal component analysis of dynamic fluorescence images for diagnosis of diabetic vasculopathy," Journal of biomedical optics, vol. 21, p. 046003, 2016.

[22]. Ntziachristos V, Yodh AG, Schnall M, and Chance B, "Concurrent MRI and diffuse optical tomography of breast after indocyanine green enhancement," Proc Natl Acad Sci U S A, vol. 97, pp. 2767–72, 3 14 2000. [PubMed: 10706610]

[23]. Lin Y, Thayer D, Nalcioglu O, and Gulsen G, "Tumor characterization in small animals using magnetic resonance-guided dynamic contrast enhanced diffuse optical tomography," J Biomed Opt, vol. 16, p. 106015, 10 2011. [PubMed: 22029362]

[24]. Unlu MB, Birgul O, and Gulsen G, "A simulation study of the variability of indocyanine green kinetics and using structural a priori information in dynamic contrast enhanced diffuse optical tomography (DCE-DOT)," Phys Med Biol, vol. 53, pp. 3189–200, 6 21 2008. [PubMed: 18506072]

[25]. Hillman EM and Moore A, "All-optical anatomical co-registration for molecular imaging of small animals using dynamic contrast," Nat Photonics, vol. 1, pp. 526–530, 2007. [PubMed: 18974848]

[26]. Bruns OT, Bischof TS, Harris DK, Franke D, Shi Y, Riedemann L, et al., "Next-generation in vivo optical imaging with shortwave infrared quantum dots," Nature biomedical engineering, vol. 1, p. 0056, 2017.

[27]. Mohajerani P, Meier R, Noël PB, Rummeny EJ, and Ntziachristos V, "Spatiotemporal analysis for indocyanine green-aided imaging of rheumatoid arthritis in hand joints," Journal of biomedical optics, vol. 18, p. 097004, 2013. [PubMed: 24045692]

[28]. Welsher K, Sherlock SP, and Dai H, "Deep-tissue anatomical imaging of mice using carbon nanotube fluorophores in the second near-infrared window," Proceedings of the National Academy of Sciences, vol. 108, pp. 8943–8948, 2011.

[29]. Wang X and Paliwal KK, "Feature extraction and dimensionality reduction algorithms and their applications in vowel recognition," Pattern recognition, vol. 36, pp. 2429–2439, 2003.

[30]. Park HJ, Griffin RJ, Hui S, Levitt SH, and Song CW, "Radiation-Induced Vascular Damage in Tumors: Implications of Vascular Damage in Ablative Hypofractionated Radiotherapy (SBRT and SRS)," Radiation Research, vol. 177, pp. 311–327, 2012/03/01 2012. [PubMed: 22229487]

[31]. Kim M-S, Kim W, Park IH, Kim HJ, Lee E, Jung J-H, et al., "Radiobiological mechanisms of stereotactic body radiation therapy and stereotactic radiation surgery," Radiation oncology journal, vol. 33, pp. 265–275, 2015. [PubMed: 26756026]

[32]. Judd NP, Allen CT, Winkler AE, and Uppaluri R, "Comparative analysis of tumor-infiltrating lymphocytes in a syngeneic mouse model of oral cancer," Otolaryngology–Head and Neck Surgery, vol. 147, pp. 493–500, 2012. [PubMed: 22434099]

[33]. Lin Y, Barber WC, Iwanczyk JS, Hartsough NE, Roeck W, Nalcioglu O, et al., "Quantitative fluorescence tomography using a combined tri-modality FT/DOT/XCT system," Optics Express, vol. 18, pp. 7835–7850, 2010. [PubMed: 20588625]

[34]. Nouizi F, Kwong TC, Ruiz J, Cho J, Chan Y-W, Ikemura K, et al., "A thermo-sensitive fluorescent agent based method for excitation light leakage rejection for fluorescence molecular tomography," Physics in medicine and biology, 2018.

[35]. Dogdas B, Stout D, Chatziioannou AF, and Leahy RM, "Digimouse: a 3D whole body mouse atlas from CT and cryosection data," Phys Med Biol, vol. 52, pp. 577–87, 2 7 2007. [PubMed: 17228106]

[36]. Song CW, Lee Y-J, Griffin RJ, Park I, Koonce NA, Hui S, et al., "Indirect tumor cell death after high-dose hypofractionated irradiation: implications for stereotactic body radiation therapy and stereotactic radiation surgery," International Journal of Radiation Oncology Biology Physics, vol. 93, pp. 166–172, 2015.

[37]. Dehlholm C, Brockhoff PB, and Bredie WL, "Confidence ellipses: A variation based on parametric bootstrapping applicable on multiple factor analysis results for rapid graphical evaluation," Food Quality and Preference, vol. 26, pp. 278–280, 2012.

[38]. Oweida A, Phan A, Vancourt B, Robin T, Hararah MK, Bhatia S, et al., "Hypofractionated Radiotherapy Is Superior to Conventional Fractionation in an Orthotopic Model of Anaplastic Thyroid Cancer," Thyroid, vol. 28, pp. 739–747, 2018/06/01 2018. [PubMed: 29774792]

[39]. Martin OA, Anderson RL, Russell PA, Ashley Cox R, Ivashkevich A, Swierczak A, et al., "Mobilization of Viable Tumor Cells Into the Circulation During Radiation Therapy," International Journal of Radiation Oncology*Biology*Physics, vol. 88, pp. 395–403, 2014/02/01/2014.

[40]. Martin OA, Anderson RL, Narayan K, and MacManus MP, "Does the mobilization of circulating tumour cells during cancer therapy cause metastasis?," Nature Reviews Clinical Oncology, vol. 14, p. 32, 08/23/online 2016.

[41]. Camphausen K, Moses MA, Beecken W-D, Khan MK, Folkman J, and O'Reilly MS, "Radiation Therapy to a Primary Tumor Accelerates Metastatic Growth in Mice," Cancer Research, vol. 61, p. 2207, 2001. [PubMed: 11280788]

[42]. Bodo S, Campagne C, Thin TH, Higginson DS, Vargas HA, Hua G, et al., "Single-dose radiotherapy disables tumor cell homologous recombination via ischemia/reperfusion injury," J Clin Invest, vol. 129, pp. 786–801, 2 1 2019. [PubMed: 30480549]

[43]. Budach W, Taghian A, Freeman J, Gioioso D, and Suit HD, "Impact of stromal sensitivity on radiation response of tumors," J Natl Cancer Inst, vol. 85, pp. 988–93, 6 16 1993. [PubMed: 8496984]

[44]. Torok JA, Oh P, Castle KD, Reinsvold M, Ma Y, Luo L, et al., "Deletion of Atm in Tumor but not Endothelial Cells Improves Radiation Response in a Primary Mouse Model of Lung Adenocarcinoma," Cancer Res, vol. 79, pp. 773–782, 2 15 2019. [PubMed: 30315114]

[45]. Castle KD and Kirsch DG, "Establishing the Impact of Vascular Damage on Tumor Response to High-Dose Radiation Therapy," Cancer Research, p. canres.13232019, 2019.

[46]. Zahra MA, Hollingsworth KG, Sala E, Lomas DJ, and Tan LT, "Dynamic contrast-enhanced MRI as a predictor of tumour response to radiotherapy," The lancet oncology, vol. 8, pp. 63–74, 2007. [PubMed: 17196512]

[47]. Rafat M, Ali R, and Graves EE, "Imaging radiation response in tumor and normal tissue," American journal of nuclear medicine and molecular imaging, vol. 5, p. 317, 2015. [PubMed: 26269771]

[48]. Clark D and Badea C, "Micro-CT of rodents: state-of-the-art and future perspectives," Physica medica, vol. 30, pp. 619–634, 2014. [PubMed: 24974176]

[49]. Kasoji SK, Rivera JN, Gessner RC, Chang SX, and Dayton PA, "Early assessment of tumor response to radiation therapy using high-resolution quantitative microvascular ultrasound imaging," Theranostics, vol. 8, p. 156, 2018. [PubMed: 29290799]

[50]. LINDBLOM EK, Hui S, Brooks J, Dasu A, KUJAWSKI M, and TOMA-DASU I, "Radiation-induced Vascular Damage and the Impact on the Treatment Outcome of Stereotactic Body Radiotherapy," Anticancer research, vol. 39, pp. 2721–2727, 2019. [PubMed: 31177107]

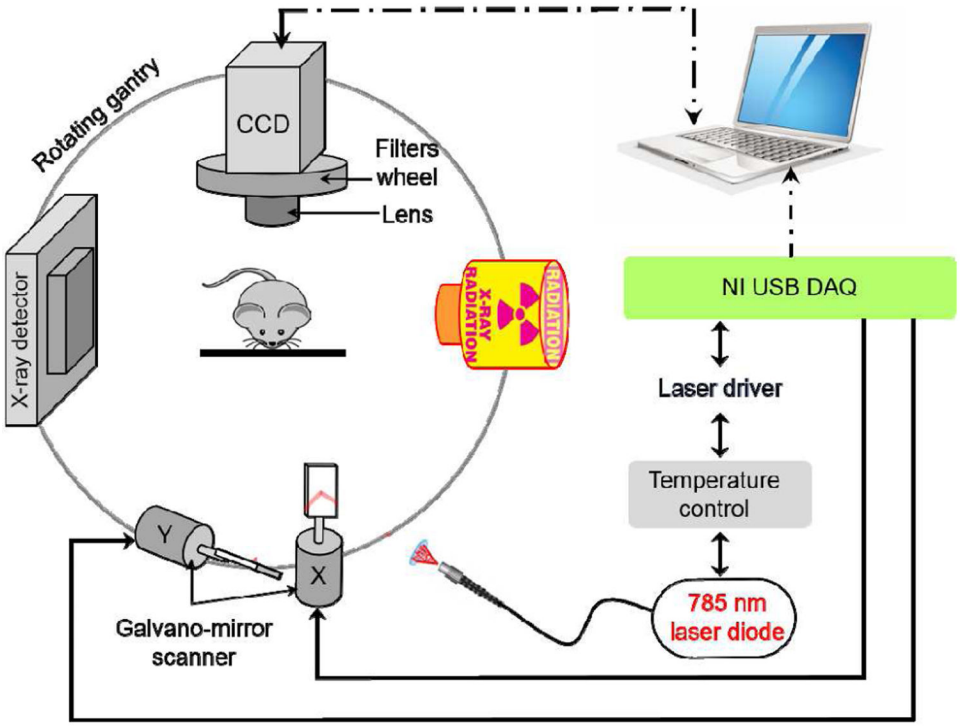

Fig. 1.

Diagram of the theranostic system. The X-ray source is used to both perform CT imaging and high-dose irradiation. For DynFI, a CCD camera is positioned above the mouse while it is illuminated from below using a 785 nm laser and an XY Galvano-mirror scanner. A temperature control unit is used to maintain the laser operating temperature. NI USB DAQ: National Instrument USB data acquisition card. The dashed lines indicate USB connections.

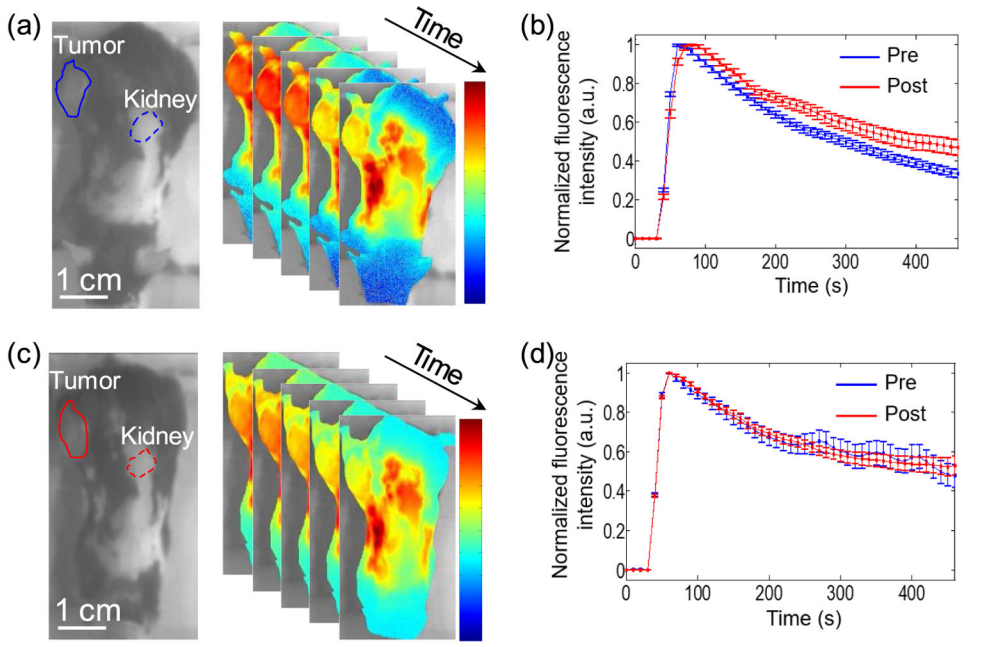

Fig. 2.

Representative ICG Kinetics pretreatment (a) and posttreatment (c) gray scale ambient-light images (left) and DynFI images acquired at 40 s, 60 s, 130 s, 350 s, and 450 s superimposed onto gray scale ambient-light images (right). DynFI images are presented using a logarithmic-scale for better visualization. Ambient-light images (left) show the locations of the tumor ROI (solid-line) and the kidney ROI (dashed-line) used for analysis. The red dot represents the position of the transilluminated laser excitation source. The plotted mean fluorescence intensity values of DynFI data for the tumor ROI (b) and the kidney ROI (d) for pretreatment (blue) and two days posttreatment(red). Error bars represent standard deviation.

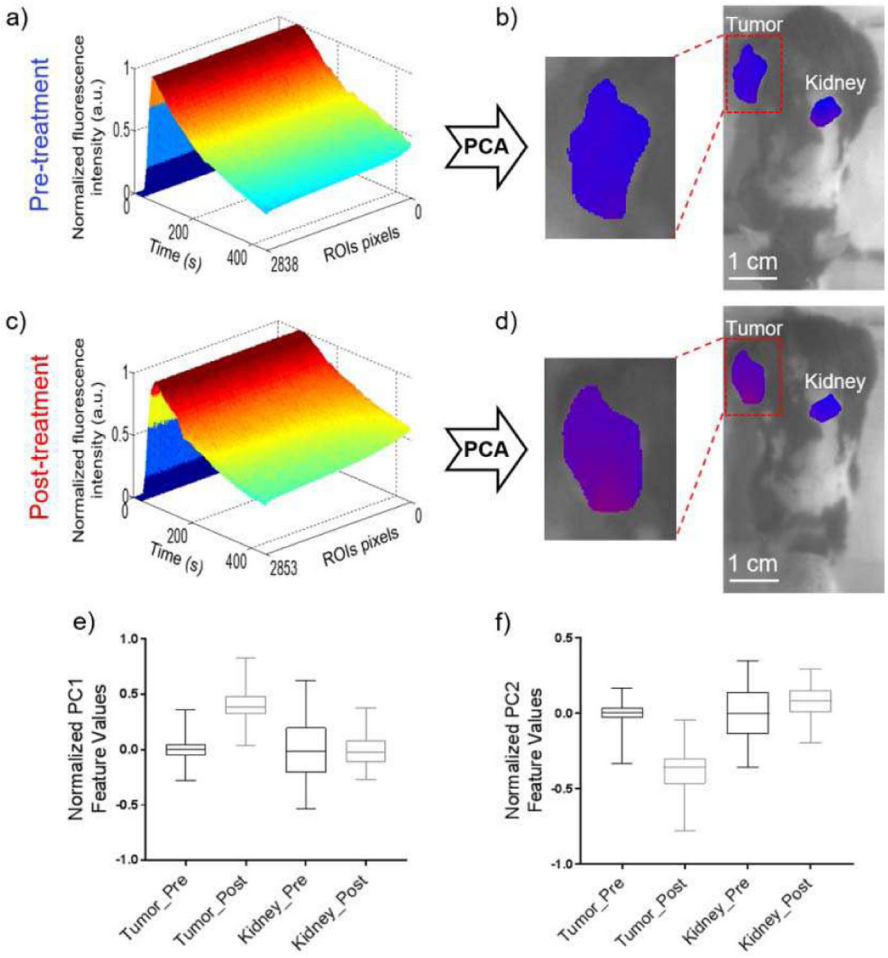

Fig. 3.

PC feature-based analysis of the DynFI data obtained from the mouse shown in Fig. 2. Normalized time-series of ICG fluorescence intensity for all individual pixels in the pretreatment tumor ROI (2838 pixels) (a) and the two days posttreatment tumor ROI (2853 pixels) (c). PC-RGB images of normalized PC1 and PC2 feature values superimposed on ambient-light images are shown before (b) and two days after (c) 10Gy SBRT treatment. The normalized PC1 and PC2 feature values were assigned to the red and blue channels, respectively. Green intensities were set to zero. A clear change from blue to red can be seen from pretreatment to two days posttreatment, showing TVR. Box and whisker plots of normalized PC feature values for PC1 (e) and PC2 (f) tumor and kidney ROIs from the corresponding pretreatment and two days posttreatment DynFI data. An increase in normalized PC1 feature values and a decrease in normalized PC2 feature values are seen in the tumor posttreatment, while no change is seen for kidney.

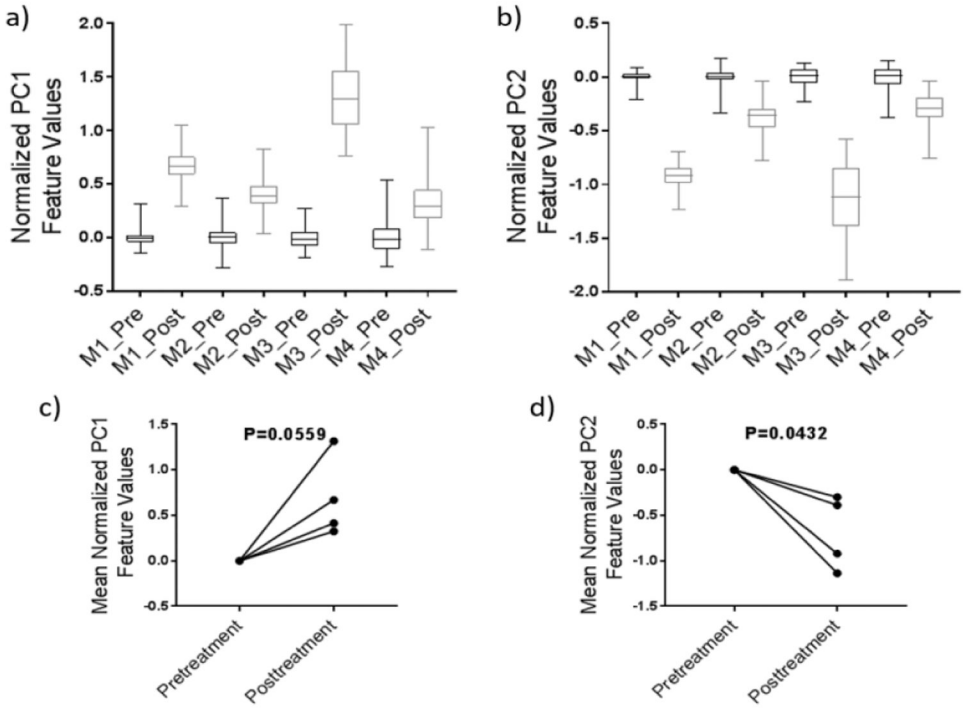

Fig. 4.

Box and whisker plots comparing the pre and two days posttreatment normalized PC1 (a) and PC2 (b) feature values for all four mice. The mean whole-tumor normalized PC1 (c) and PC2 (d) tissue values are shown along with the corresponding paired t-test.

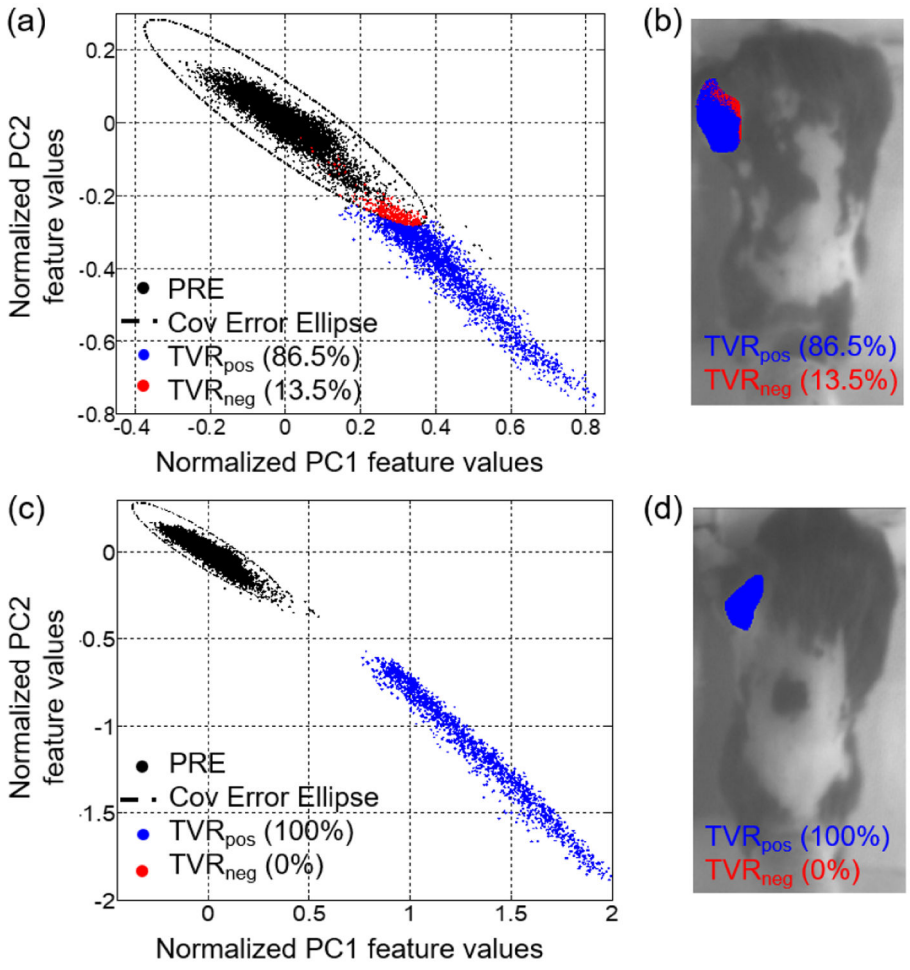

Fig. 5.

Automated classification of TVR using a confidence covariance Ellipse algorithm. Scatter plots of normalized PC1 and PC2 feature values for mouse two (a) and mouse three (c) are shown. The normalized PC feature values from pretreatment images (PRE) are shown as black dots. The classification algorithm calculated a 99.9% confidence covariance ellipse (dashed line) from pretreatment data, which was used to classify the posttreatment pixels as TVR_{pos} (blue) and TVR_{neg} (red). Ambient-light posttreatment images of mouse two (b) and mouse three (d) with the overlaid tumor ROI pixels classified as TVR_{pos} (blue) and TVR_{neg} (red) are shown.